MICROSCOPY AND MOSSBAUER STUDIES OF IRON STATES IN DOPED GALIUM ANTIMONIDE

C. Turta[1,*], V. S. Teodorescu[2], A. Mihalache[3,*], E. Gheorghitsa[3], G.F. Volodina[4], and G. Filoti[2]

[1]*Institute of Chemistry, Academy of Sciences of Moldova, Academiei str. 3, Chisinau, MD 2028 Republic of Moldova, turtalcba@gmail.com*

[2]*National Institute of Materials Physics, 105 bis, Atomistilor str., Bucharest, Magurele, P.O. Box MG-7, Ro-077125 Romania, filoti@infim.ro*

[3]*Tiraspol State University, Moldova, Iablocichin str. 5, Chisinau, MD 2069 Republic of Moldova, alexei.mihalache@gmail.com*

[4]*Institute of Applied Physics, Academy of Sciences of Moldova, Academiei str. 5, Chisinau, MD 2028 Republic of Moldova*

(Received December 30, 2013)

Abstract

A single crystal of gallium antimonide doped with 3 at % ^{57}Fe was obtained via the Czochralski method. The Mössbauer investigations revealed four iron patterns: one diamagnetic and three Fe magnetically ordered sites, even at room temperature. The data suggested that iron-containing compounds are formed at grain boundaries, and the microscopy images revealed the presence of two types of boundaries and holes of different shape and size. The EDX spectrum provided different amounts of Fe in the crystal (GaSb) and, respectively, at the boundary area.

1. Introduction

Gallium antimonide (GaSb) is one of binary semiconductors with a narrow energy bandwidth, a low electron effective mass, and a high mobility. It is a material with crystal lattice and adequate parameters of semiconducting properties suitable for building optoelectronic devices in a range of 0.8–4.3 μm [1–3]. The influence of doping elements belonging to the 3d transitional metals Fe, Ni, Cr, and Mn in the binary semiconductors, for instance, gallium antimonide, on the new physical properties is of high relevance. Among other trends, of a special interest is the preparation of magnetic materials with polarized electrons in a high spin state, which are referred to as dilute magnetic semiconductors (DMSs) [4]. The most obvious advantage of these materials consists in the possibility to implement magnetic storage of information with electronic readout in a single semiconductor device. As was demonstrated in [5], the spin injection may be carried out when electrochemical potentials in the ferromagnets will be split and the resistance of the ferromagnet is of comparable magnitude to the contact resistance. Thorough studies of the Fe–Ga system function on the component ratios and temperature resulted in the publication of the state diagrams of alloys indicating stable intermetallic compounds and their compositions [6, 7]. The main intermetallic substances obtained are: the cubic α-Fe_3Ga, Pm3m space group, in a range of 20.6–26.3 at % Ga having the

solidification temperature of T_c = 588°C; the hexagonal β-Fe_3Ga, space group $P6_3/mm\bar{c}$, exists in the limits of 24.3–32.0 at % Ga and crystallizes between 590-700°C; the monoclinic or tetragonal Fe_3Ga_4 with composition in at % Ga between 56.5–58.0, the space group C2/m, has a peritectic formation temperature of 906 ± 2°C; the β-Fe_6Ga_5, R3m space group, containing ~45 at % Ga, exists in a narrower temperature range of 770–800°C; the α-Fe_6Ga_5, with the same composition, which is characterized by C2/m space group and is stable at temperatures below 770°C; and finally the tetragonal $FeGa_3$, space group P4n2.

According to [8, 9], the Fe-Sb phase diagram consists of two phases: stoichiometric $FeSb_2$ and $Fe_{1+x}Sb$. The $FeSb_2$ component is stable in the limits of 45–67 at % Sb at temperatures below 738°C. The space group of the monocrystal is Pnn2 (FeS_{2-m} type structure) [10]. Each Fe atom is situated in interstitial sites of Sb atoms and surrounded by six Sb atoms, while the Sb atom is surrounded by three nearer iron atoms and one antimony atom. The structure of $FeSb_2$ does not change at lower temperatures (4–80 K), but the quadrupole splitting is changed; FeSb is crystallized in a range of 42–48 at % Sb in the $B8_1$ structure type. The antimony atoms form a hexagonal close-packed lattice, and the iron atoms are situated either in octahedral or tetrahedral interstices [11]. The NiAs-type $B8_1$, the phase Fe_3Sb_2(ε), has a homogeneity range of 40–47 at % Sb with maximum liquid curve at 1025°C [12].

The role of doping atoms in semiconductors could be evidenced via indirect and direct experimental methods. The most ordinary (indirect) methods to investigate the role of doping atoms in a semiconductor host involve measurements of electrical conductivity, galvanomagnetic effects, photo conductibility, thermoelectric force, etc. These methods used in the investigation of semiconductor materials provide the biggest portion of information about the role and state of enclosed atoms in semiconductors. However, the interpretation of data concerning the location of these centers, which can be substitutional, interstitial, and located at the limit of the grain or on the vacancy places, requires great caution and finally is based on results obtained by direct methods, such as electronic paramagnetic resonance (EPR), nuclear magnetic resonance (NMR), nuclear quadrupole resonance (NQR), nuclear gamma resonance (Mössbauer spectroscopy, MS), X-ray photoelectron spectroscopy (XPS), perturbed angular correlations (PAC), etc. However, these methods are not universal, such as electrical conductivity or Hall Effect measurements; therefore, they are applicable to a limited number of semiconductors (containing accessible isotopes in the case of NMR and Mössbauer, valence and spin state for EPR) or to a restricted set of impurities, enclosed atom present in them. The role of electronic paramagnetic resonance spectroscopy method to justify the basics of the theory of doped centers in semiconductors is well known [13, 14].

During recent years, the specific literature has accumulated a significant amount of data on doped centers in Fe–Ga and Fe–Sb systems and III-V semiconductors obtained by Mössbauer spectroscopy [15-23]. In [24], the spin injection at room temperature by introducing of Fe_3Si epitaxial layer into GaAs matrix was successfully demonstrated. This result represents an example of ferromagnetic Heusler alloy (Fe_2FeSi) which is a case of favorable spin injection. Considering that the solubility of doping III-V semiconductors is effectively small, in order to surpass the difficulties, it was chosen to work far from equilibrium by using epitaxial molecular flow (EMF) at low temperatures. For the GaAs system, Curie temperature T_c values of 60 [25] and 159 K [26] were obtained. Upon switching to broadband semiconductors, GaN and ZnO, the T_c values were significantly increased. Thus, in [27] T_c above 740 K was obtained by 3% Mn doping in a GaN matrix on an Al_2O_3 support. A theoretical study [28] showed that Cr and Mn dopants in the cubic 3C-SiC polytype produce a ferromagnetic solid solution for both C and Si

position, exhibiting different magnetic moments. Implantation of Fe in SiC did not lead to magnetic phase, but the replacement of silicon (Si) by iron (Fe) (at low concentrations) in the hexagonal H_6SiC polytype changed the crystal into a ferromagnetic phase. The electrical and optical properties of specified devices are widely affected by the doping material, usually owing to the diffusion of the desired element into the semiconductor crystal [29]. The actual study reports on the growth of a p-type gallium antimonide doped with 3 wt % ^{57}Fe, the related optical and TEM images, and a large set of data obtained using ^{57}Fe Mossbauer spectroscopy performed at different temperatures (3–295 K).

2. Material and methods

Sample synthesis: Amounts of Ga, *m* = 0.6545 g; Sb, *m*= 1.4250 g; and ^{57}Fe, *m* = 0.0331 g were loaded into an optical quartz ampoule with thick walls (2–3 mm) and an internal diameter of ~12 mm. The evacuation of the atmosphere alternates with a few cycles of washing with argon. At the residual gas pressure of 10^{-5} mm Hg, the ampoule containing sample was sealed and tightly connected to an electromagnetic vibrator (50 Hz) to provide a homogeneous mixture. Both the ampoule and the vibrator were placed inside a tube type furnace. A constant temperature of 900°C was maintained for 24 h. After that, the electrical supply was switched off and the furnace was freely cooled via its thermal inertia. The obtained product was ground into a powder and then introduced into the zone melting facility to grow a single crystal via the Czochralski method. A mass of 0.040 g was separated from the grown single crystal, ground into a very fine powder and used as a sample (placed in a specific holder) for Mossbauer measurements.

Mössbauer measurements. The Mössbauer spectra were measured via Oxford Instruments Mössbauer-Spectromag 4000 Cryostat from Institute of Inorganic Chemistry, Karlsruhe University. The temperature was varied within 3.0–300 K. A ^{57}Co source (3.7 GBq) in a rhodium matrix was used. The spectrometer was of the electrodynamic type with a constant acceleration symmetrical waveform. Isomer shifts values are referred to Fe-metal at room temperature. The fits of the experimental data were performed using the wmoss and NORMOSS programs.

X-ray diffraction measurements (XRD) of powder were realized at the Institute of Applied Physics of the Academy of Sciences of Moldova via DPOH-УМ1 equipment. (FeK_α-radiation, Mn filter, $\theta/2\theta$ method.).

Transmission electron microscopy (TEM) images were recorded using a Jeol ARM 200F electron microscope. The ion thinning was performed using a Gatan PIPS model 691 device operating at 5 kV and 6 degrees incidence. Optical images were obtained using an AXIO-Zeiss-ObserverA1m microscope. For TEM specimen preparation, a slice with a thickness of about 500 μm was cut parallel to the basal plane from the cylindrical GaSb crystal sample, using diamond wire devices. In the second step, the slice was cut in nine smaller pieces. Finally, the 0.5 mm x 2 mm x 2 mm GaSb piece was mechanically polished on both faces until a thickness of about 30 μm and glued on a 3-mm copper TEM grid. This grid was then ion thinned to obtain a small hole in the middle. The edges of this hole are transparent to the electron beam in the microscope. The TEM specimen was oriented with the microscope axis parallel with the cylindrical axis of the initial cylindrical GaSb sample.

3. Results and discussion

Galium antimonide doped with Fe-57 isotope studied in this paper was obtained as described in "Materials and Methods." The Mössbauer spectra (MS) of GaSb-Fe sample (3 at % Fe-57) at different temperatures are presented in Fig. 1.

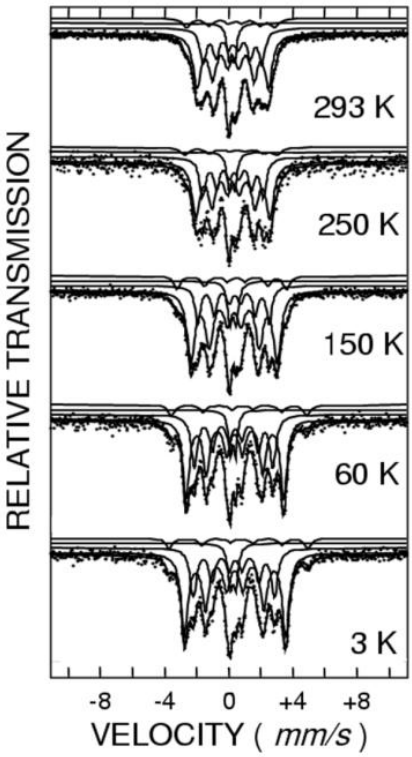

Fig. 1. Mössbauer spectra of GaSb-Fe sample (3 at % Fe-57) at different temperatures.

At a first glimpse, the most remarkable aspect of the spectra is the existence at a fairly high temperature of 298 K (RT = room temperature) of three six-line patterns, suggesting the magnetic species for three iron locations. These sextets, also the centrally placed doublet, appeared over the entire temperature range (3–295 K) of Mössbauer measurements. The Mössbauer spectra parameters of investigated sample are presented in Table 1.

It is remarkable that the values (last column in the table) of relative area (proportional to the amount of Fe ions on every of its location) remain in reasonable limits.

The presence of four different patterns in all exhibited Mössbauer spectra draw attention to a very important experimental feature. A homogeneous distribution of only 3 at % enriched ^{57}Fe inside the GaSb single crystal lattice (zinc blend cell), substituting either the Ga or Sb atoms, normally would provide two doublets corresponding to both tetrahedral surroundings of Ga and of Sb and showing identical distances to the nearest neighbors of different type and to the second sphere of 12 neighbors of the same type as the central ion of the coordination. In this case, both the IS and QS will show distinct figures due to a peculiar bond of Fe with Ga and, respectively Sb, with higher values for Fe location on Ga sites. Previous attempts of doping with Mn (for example, Mn in GaSb [30]) have failed to prove any substitution location. Therefore, the presence of Fe in four sites suggests the formation of potentially well crystallized (preparation route) of binary or ternary type compounds. These phases could exist mainly or only at dislocation or packing defects appearing during the growth of the single crystal. These dislocations are developed

preponderantly at the surface of the crystal and evolve inside the crystal, function of processing temperatures and the stress induced by growing.

Table 1. Mössbauer spectra parameters of the GaSb–Fe sample at different temperatures

T(K)	Compo-nents	B_{eff} (T*)	mm/s			A (%)
			QS	IS	W	
3	1	19.5	0.03	0.48	0.56	56
	2	15.7	-0.10	0.48	0.57	30
	3	0.0	0.34	0.39	0.36	8
	4	26.8	-0.22	0.51	0.27	6
60	1	18.8	0.03	0.48	0.47	52
	2	15.2	-0.10	0.47	0.47	34
	3	0.0	0.33	0.38	0.28	7
	4	26.2	-0.21	0.48	0.47	7
150	1	16.7	-0.02	0.45	0.57	59
	2	13.8	-0.07	0.44	0.41	22
	3	0.0	0.39	0.37	0.36	10
	4	21.1	-0.26	0.44	0.39	9
250	1	14.3	-0.03	0.39	0.57	53
	2	11.8	-0.07	0.41	0.46	30
	3	0.0	0.37	0.32	0.32	8
	4	17.9	-0.32	0.40	0.46	9
293	1	13.8	-0.04	0.38	0.58	54
	2	11.4	-0.04	0.37	0.48	29
	3	0.0	0.32	0.31	0.32	8
	4	17.0	-0.23	0.36	0.56	9

B_{int} is the internal magnetic field around the iron nucleus, error = ± 0.2 T; QS is the quadrupole splitting, IS is the isomer shift, W is the full line width, errors of QS, IS, W = ± 0.02 mm/s; A is the relative area, error = ± 1 %; T* is Tesla).

Another significant feature is the continuous decrease of the IS with temperature proving the effect of second order Doppler shift [31].

The assignation of the patterns was related to Mössbauer existing data from the literature and their analyses in terms of temperature and composition dependence of corroborated parameters.

According to the phase diagram (600°C) of ternary FeGaSb system presented in Fig. 1 of [12, 32] and phase diagrams of Fe–Ga and Fe–Sb [7, 8], at low iron concentrations, the FeGaSb system can contain the following phases: FeSb, $FeSb_2$, Fe_3Sb_2 (ε), Fe_3Ga, Fe_6Ga_5, Fe_3Ga_4, $FeGa_3$, and epitaxial iron particles at nanoscale [33, 34].

The most facile choice was for the doublet case. Comparing the experimental values of Mössbauer spectra parameters for doublet (component 3) of the sample at RT (IS = 0.31 mm/s, QS = 0.32 mm/s) (Table 1) with the literature data for MS doublets of Fe–Sb and Fe–Ga systems [15–17, 34–37] at the same temperature, one can see that they are closest to the diamagnetic $FeGa_3$ [38] (IS = 0.28, QS = 0.31 mm/s [37]). Checking the structures, the XRD diffractograms (Figs. 2a, 2b) confirm the presence of this compound.

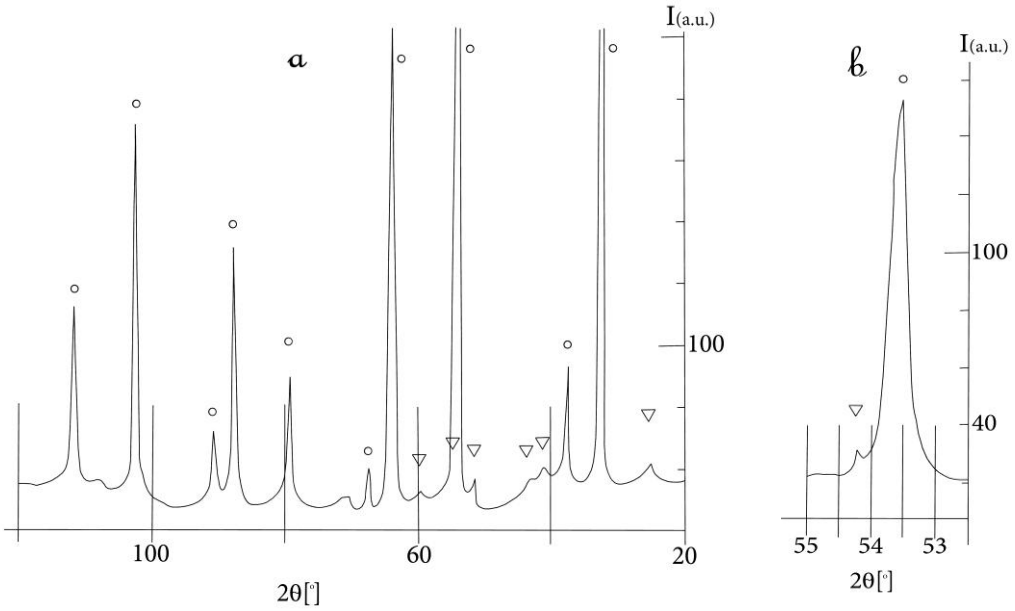

Fig. 2. (a) X-Ray powder diffraction spectra of investigated sample GaSb-Fe (3%): o—spectrum peaks for GaSb, ▽ —peaks for $FeGa_3$ substance and (b) line separation 220 GaSb (d = 2.156 Å) and 212 FeGa3 (d = 2.126 Å).

There have been as well other possibilities for a paramagnetic component; among the first of them, it was the presence of $FeSb_2$. However, in the actual case, it has to be completely excluded because the experimental values of QS (MS) are about 4 times lower (Table 1) than those reported in [15, 17, 18, 39] with values of QS = 1.26–1.29 mm/s and IS = 0.46–0.45 mm/s at RT.

Another alternative was amorphous a-$FeSb_2$ or more close in values of IS and QS the amorphous compound $Fe_{0.5}Sb_{0.5}$ [17] with QS = 0.44; 0.51 mm/s and IS = 0.43, 0.54 mm/s at RT and 4.2K, respectively, but these compounds are definitely out of any consideration, due to the process of growing single crystals. The data of $Fe_{1.3}Sb$ [40, 41] point to a doublet at RT but shows two sextets: one very pronounced, with B_{int} around 11–12 T, and the other one close to 16–17 T at 5 K; therefore, they are not suitable for our doublet assignation.

As specified above, the studied sample contains three sextet components (labelled 1, 2, 4) with different values of internal magnetic field B_{int} equal to 13.8 T (1), 11.4 T (2) and 17.0 T (4) at 293 K. Note that these values are much lower than that characteristic of α-Fe (B_{int}, 33 T), indicating the formation of systems with the composition $Fe_3(Ga_{1-x}Sb_x)_2$ [19, 20] or Fe_3Ga_4 [42], as well Fe_3Ga or $Fe_{1+x}Sb$ [40, 41], where x may cover a large range of values. It is worth noticing that, from the beginning, the formation of a Fe_3Ga_4 compound, where 4 sextets are observed and related IS values are close to zero, was excluded [42],. The $Fe_{1-x}Ga_x$ alloys were studied in [43],

with $0.15 \leq x \leq 0.30$. Those samples, obtained by ball milling, were studied by X-ray powder diffraction, magnetization, electroconductibility, and Mössbauer spectroscopy methods in a large temperature interval of 5–770 K. The XRD data demonstrated the presence of three crystallographic phases: α (Disorder (bcc)), stable within 15 to 20 at % Ga; α" (Order (bcc), $FeAl_3$-DO_3), stable within 20-30 at.% Ga; and β (Order (fcc), Cu_3Au=LI_2) stable within 25–30 at % Ga. Curie temperature T_c, magnetic moment μ (μB) /atom, B_{int}, IS, QS, and electroresistivity were determined. Later, close data were published in [44] for $Fe_{100-x}Ga_x$, where x = 15.7, 17.0, 19.0, 22.4, and 24.0, which was obtained by ball milling. In both cases, the values of B_{int}, IS, and QS differ from our data.

For all magnetic components of here investigated sample, the Curie temperatures T_c are higher than 293 K and in good agreement with the literature data. For example, in ternary systems $Fe_3(Ga_{1-x}Sb_x)_2$ and $Fe_3Ga_{2-y}As_y$, where $0.1 \leq x \leq 0.75$; $0.21 < y < 1.125$, it was demonstrated by various physical methods that the magnetic ordered state with T_C quite high up to 360–374°C is present and magnetic properties strongly depend on the proportion of Ga and Sb amount surrounding the Fe [19, 20, 35, 36]. In one attempt to assign the observed three magnetically ordered components of the investigated sample, we mainly used the results reported for $Fe_3Ga_{2-x}M_x$. According to [20, 35], the $Fe_3(Ga_{1-x}Sb_x)_2$ systems, as well as $Fe_3(Ga_{1-x}As_x)_2$, have the $B8_2$ hexagonal structure type belonging to the P63/mmc space group, which is characteristic of the Ni_2In type. In this structure, there are two positions of Ni ions: with octahedral (Oh, $NiIn_6$) environment and one asymmetrical $NiIn_5$ environment. It is obvious that the 1st and 2nd sextets should belong to the octahedral environment (lower values of QS parameter), while the 4th sextet to asymmetrical. As stated above, the most important approach in our analyses was the effect of presence of various elements from pnictide group on B_{int}, IS, and eventually QS parameters in Fe_3Ga_2 systems. From this point of view, the data from [20, 35] suggest a composition rather poor in Sb and richer in Ga in direct relation with reported data in [20]. In fact, Table 9 in [20] revealed that, with decreasing Sb content from x = 1 to x = 0.3, the B_{int} (at RT) augments by 1.5–1.7 T. Extrapolating the RT values found for the two octahedral surroundings in our study (Table 1), the observed patterns could stand for a composition with 0.10–0.15 Ga and 1.90 or 1.85 Sb. In the study of Smith et al. [20], a composition with x = 0.10 (T_C data with values around 375 K) was prepared; however, any Mössbauer spectrum or parameters were not provided.

The Mössbauer line widths W (Table 1) for the sextets of all three positions are fairly large compared to the line width measured with our source and a standard alpha-Fe absorber (W = 0.25 mm/s). The large line width may be assumed to be an effect of the tiny modified nonequivalent surroundings and to relaxation processes. It should be noted that the mentioned components of the GaSb–Fe system are not formed via substitutions of either Ga or Sb in the GaSb single crystal, but are formed at the boundary; hence, their influence on the magnetic, electrical, and other properties will be peculiar. Starting to elucidate the above statements, the optical and electron microscopy measurements were envisaged.

The reflection optical image of the "as prepared" TEM specimen is shown in Fig. 3. Two types of crystal domains are observed (transparent and grey) exhibiting large boundaries between them. The optical contrast is due to the ion beam etching for the different crystallographic orientations of the two types of the domains. The areas near the edges of the black hole situated in the middle of the image in Fig. 3 are transparent areas for the electrons in the microscope. Figure 4 shows a TEM image obtained in these transparent areas representing the GaSb mono crystal structure in the <111> orientation demonstrated by the electron pattern inserted in the

figure. The arrows in Fig. 4 show the presence of Ga precipitates on the surface of the GaSb TEM specimen after several minutes of observations under the electron beam irradiation being formed by diffusion of this element from the bulk.

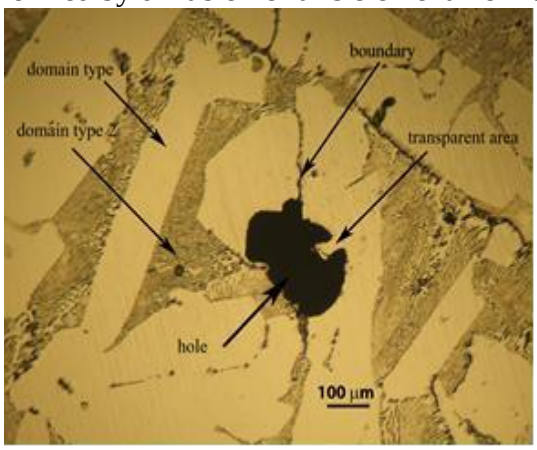

Fig. 3. Optical image (in reflection) of the axis the GaSb-Fe TEM specimen.

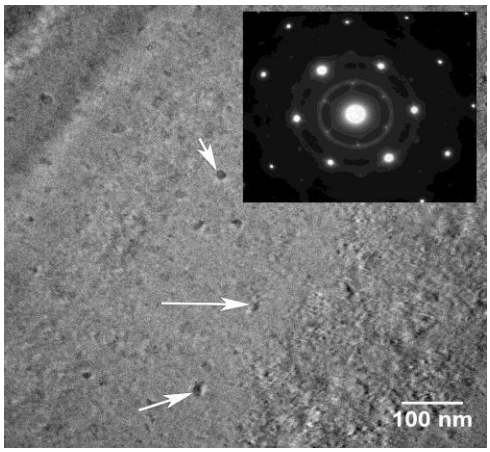

Fig. 4. Domain oriented in the <111> zone of the cubic GaSb structure.

As shown (Fig. 5) in the energy dispersive X-ray spectra (EDX), the Fe amount in the crystal bulk areas is less than 0.3 at %, while in the thick area (Fig. 6) of the specimen obtained from the location on the boundaries, about 2.5% Fe is present. The excess Ga concentration observed in the thin areas of the TEM specimens has two causes. The first one is the ion thinning process, which changes the sample concentration near the exposed surface, and the second one is the electron irradiation in the microscope, which enhances the Ga diffusion on the TEM specimen surface. After several minutes of observations, nanometric precipitates of Ga appear on the specimen surface, (see Fig. 4). In the thick areas of the TEM specimen, the Ga and Sb concentration resulted from EDX spectra are almost equal, because the amount of the Ga on the surface is less important, comparing to the total amount of the Ga present in the bulk.

As can be observed optically, the boundary regions between the crystal domains are large (about 1 μm) and, as described above, have a larger concentration of Fe (2.5%) than in the bulk (less than 0.3%). This large boundary region, which also shows some polycrystalline structures, can be attributed to the presence of the FeGa3 structure observed by X-ray diffraction.

Due to the complex structure of the boundary region, it was impossible to obtain real transparent areas for TEM in these regions; however, EDX spectra (shown in Fig. 6) could be recorded.

These results considerably confirm and support the Mössbauer data and the related location of iron containing phases at grain boundaries. This presence indeed could not substantially influence the physical properties of the GaSb single crystal doped with a fairly small amount of Fe.

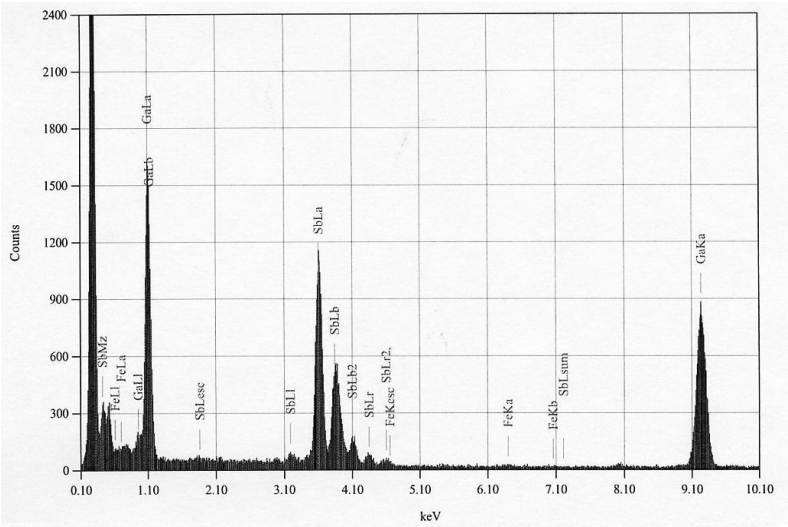

Thin Film Standardless Standard Quantitative Analysis
Fitting Coefficient : 0.5009

Element	(keV)	Mass%	Counts	Error%	Atom%	Compound	Mass%	Cation	K
Fe K	6.398	0.18	128.63	6.73	0.28				0.3986
Ga L	1.098	53.13	12874.93	0.05	66.34				1.1869
Sb L (Ref.)	3.604	46.69	13427.26	0.06	33.38				1.0000
Total		100.00			100.00				

Fig. 5. EDX spectrum from the thin transparent area of a bulk crystal after TEM observations. Ga is largely present on the specimen surface, probably due to the ion thinning process.

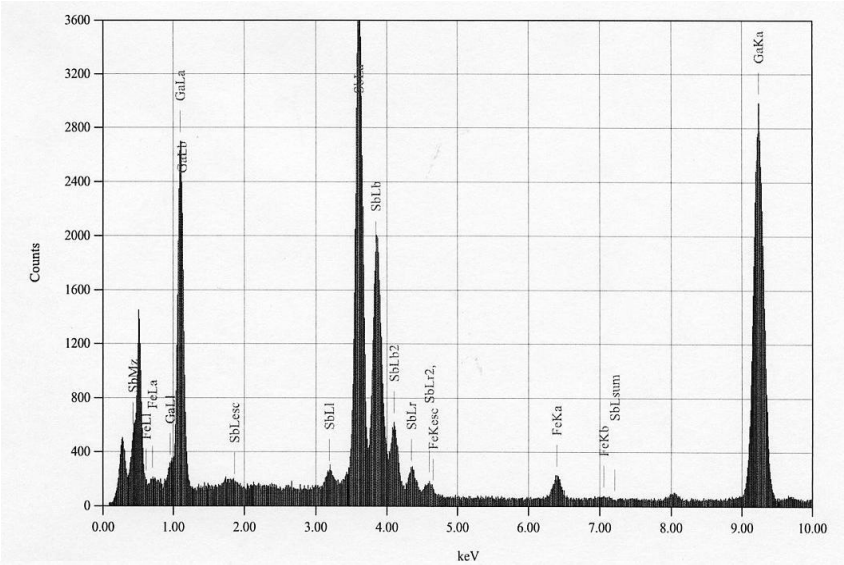

Thin Film Standardless Standard Quantitative Analysis
Fitting Coefficient : 0.2309

Element	(keV)	Mass%	Counts	Error%	Atom%	Compound	Mass%	Cation	K
Fe K	6.398	1.44	2529.94	0.13	2.46				0.3986
Ga L	1.098	34.58	20456.37	0.01	47.36				1.1869
Sb L (Ref.)	3.604	63.98	44918.98	0.01	50.18				1.0000
Total		100.00			100.00				

Fig. 6. EDX spectrum on the thick area of the specimen obtained from an area located on the boundaries between the crystal domains.

These results considerably confirm and support the Mössbauer data and the related location of iron containing phases at grain boundaries. This presence indeed could not substantially influence the physical properties of the GaSb single crystal doped with a fairly small amount of Fe.

4. Conclusions

A single crystal of GaSb doped with 3 at % Fe was prepared by the Czochralski method in order to be investigated using Mössbauer spectroscopy. The microscopy data, imperiously requested by MS results, revealed the formation of large monocrystalline domains (GaSb) with optically visible boundaries (of a few microns) and holes between them. The EDX spectrum of the boundary area granted the presence of 2.5 at % Fe concentration, while the Fe amount in the large domains of the crystal was less than 0.3 at %.

The first output from Mössbauer data was that Fe does not substitute any of the elements constituting the GaSb single crystal. The Fe is present as binary ($FeGa_3$) and ternary $Fe_3(Ga_{1-x}Sb_x)_2$ phases on the boundary sites between crystallites. Some Mössbauer parameters, such as isomer shift, line width, and fields at nucleus, are specifically influenced by the ratio between Ga and Sb in the investigated Fe-containing compounds.

References

[1] Physics of Compounds of Group IV Elements and III-V Compounds. Ed by Madelung O., Landolt-Bornstein New Series, Group 3. Mir.Moscow, 1967.
[2] A. G. Milnes and A. Y. Polyakov, Gallium antimonide device related properties, Solid-State Electron. 36, 803 (1993).
[3] P. S. Dutta, H. L. Bhat and V. Kumar, The physics and technology of gallium antimonide: An emerging optoelectronic material, J. Appl. Phys. 81, 9, 5821 (1997).
[4] H. Ohno, Making, Nonmagnetic Semiconductors Ferromagnetic, Science, 281, 5379, 951 (1998).
[5] G. Schmidt, D. Ferrand, M. Molenkamp, A. T. Filip, and van B. J. Wees, Phys. Rev. B, 62, R4790 (2000).
[6] H. Okamoto, The Fe-Ga (Iron-Gallium) system. ASM Int. Bull. Alloy Phase Diagrams, 11, 6, 576 (1990).
[7] H. Okamoto. Fe-Ga (Iron-Gallium) Section III: Suppl. Lit. Rev. J. Phase Equil. Diff. 25, 1, 100 (2004).
[8] H. Okamoto: "Fe-Sb(Iron-Antimony)" Phase Diagrams of Ternary Iron Alloys, ed., ASM International, Materials Park, OH, 366-370 (1993).
[9] K. W. Richter and H. Ioser, J.Alloys Comp., 247, 247 (1997).
[10] H. Holseth and A. Kjekshus, Acta Chimica Scand. 23, 9, 3043 (1969).
[11] M. Sladecek, M. Miglierini, B. Sepiol, H. Ipser, H. Schicketanz, and G.Vogl, Defect Diffus. Forum, 194-199, 369-374 (2001).
[12] V. Raghavan. JPEDA 25, 85 (2004) DOI:10.1361/10549710417740.1547-7037/ASMInternational.
[13] E. E. Vogel, O. Mualin, M. A. de Orue, and J. Rivera-Iratchet, Phys. Rev. B, 44, 4, 1579 (1991-II).
[14] J. E. Wertz and J. R. Bolton, Electron Spin Resonance: Elementary Theory and Practical

Applications, New York: McGraw-Hill, 1972.
[15] Ch.S. Birkel, G. Kieslich, D. Bessas, T. Claudio, R. Branscheid, U. Kolb, M. Panthofer, R.P. Hermann, and W. Tremel, Inorg. Chem.50, 11807 (2011) dx.doi.org/10.1021/ic201940r.
[16] J.M. Borrego, J.S. Blazqueza, C.F. Conde, A. Conde, and S. Rothet, Intermetallics. 15, 193 (2007).
[17] C.L. Chien, Gang Xiao, and K.M. Unruh, Phys.Rev. B, 32, 9 5582 (1985).
[18] A. Farhan, M. Reissner, A. Leithe-Jasper, and W. Steiner, J. Phys.: Conf. Ser. 217, 012142 (2010) doi:10.1088/1742-6596/217/1/012142.
[19] M. Monciardini, L. Pareti, G. Turilli, R. Fomari, A. Paoluzia, F. Albertini,O. Moze, and G. Calestani, J. Magn. Magn. Mater. 140-144, 145 (1995).
[20] N.A. Smith, P.J. Hill, E. Devlin, H. Forsyth, I.R. Harris, B. Cockayne, and W.R. MacEwan, J. Alloys Comp. 179, 111 (1992).
[21] G. Weyer, Hyperfine Interact, 177, 1 (2007). DOI10.1007/s10751-008-9607-y.
[22] R. Hu, R.P. Hermann, F. Grandjean, Y. Lee, J.B.Warren, V.F. Mitrović, and C. Petrovic, Phys. Rev. B, 76, 224422-1 (2007). doi: 10.1103/PhysRevB.76.224422.
[23] R.A. Pruitt, W. Marshall, and C.M. O'Donnell, Phys. Rev. B, 2, 7, 2383 (1970).
[24] A. Ionescu, C.A.F. Vaz, T. Trypiniotis, G.M. Gurtler, H. Garcia-Miquel, J.A.C. Bland, M.E. Vickers, R.M. Dalgliesh, S. Lanridge, Y. Bugoslavsky, Y. Miyoshi, L.F. Cohen, and K. R.A. Ziebeck, Phys. Rev. B, 71, 094401 (2005).
[25] H. Ohno, A. Shen, F. Matsukura, A. Oiwa, A. Endo, S. Katsumoto, and Y.Iye, Appl. Phys. Lett. 69, 363 (1996). http://dx.doi.org/10.1063/1.118061.
[26] C.T. Foxon, R.P. Campion, K.W. Edmonds, L.Zhao,K. Wang, N.R.S. Farley, C.R. Staddon, and B. Gallagher, J. Mater. Sci.: Mater. Electron., 15, 11, 727 (2005). doi:10.1023/BJMSE.0000043420.48864.072004.
[27] T. Sasaki, S. Sonoda, Y. Yamamoto, K. Suga, S. Shimizu, K. Kindo, and H. Hori, J. Appl. Phys. 91, 7911 (2002). dx.doi.org/10.1063/1.1451879.
[28] V.I. Shaposhnikov and N.A. Sobolev, J. Phys. Condens. Matter, 16, 1761 (2004).
[29] S.Dr. Derek, In the book: Springer Handbook of Electronic and Photonic Materials, Ed. by Safa Kasap Prof., Peter Capper Dr. 2007, Chapter 6. Diffusion in Semiconductors, pp.121-135. Doi:10.1088/0953-8984/16/10/008.
[30] A. Wolska, K. Lawniczak-Jablonska, M.T. Klepka, A. Barcz, A. Hallen, and D. Arvanitis, Acta Phys. Pol. A, 117 2, 286 (2010).
[31] R.V. Pound and G.A. Rebka, Phys. Rev. Lett. 3, 439 (1959), doi:10.1103/PhysRevLett.3.439.
[32] S. Deputier, N. Barrier, R. Guerin, and A. Guivarch, J. Alloys Comp., 340, 132 (2002.
[33] D.R.S. Somauajulu, M. Sarkar, N.V. Ptel, K.C. Sebastian, and M. Chandra, Hyperfine Interactions 136/137, 424-431 (2001).
[34] T.Yu. Kiseleva, E.E. Levin, A.A. Novakova, S.A. Kovaleva, T.F. Grigoreva, A.P. Barinova, and N.Z. Lyakhov, Proc. Tenth Israeli-Russian Bi-National Workshop 2011 "The Optimization of Composition, Structure and Properties of Metals, Oxides, Composites, Nano- and Amorphous Materials," Jerusalem, Israel, June 20-23, 2011, p.1–9.
[35] C. Greaves, E.J. Devlin, N.A. Smith, I.R. Harris, B. Cockayne, and W.R. MacEwan, J. Less Common Met. 157, 315 (1990).
[36] R. Harris, N.A. Smith, E. Devlin, B. Cockayne, W.R. MacEwan, and G. Longworth, J. Less Common Met. 146, 103 (1989).
[37] G.L. Whittle, P.E. Clark, and R. Cywinski, J. Phys. F :Metal Phys.10, 2093 (1980).

[38] K. Umeo, Y. Hadano, S. Narazu, T. Onimaru, M.A. Avila, and T. Takabatake, Phys. Rev. B, 86, 144421 (2012).
[39] J. Steger and E. Kostiner, J. Solid State Chem. 5, 131 (1972).
[40] P.J. Picone and P.E. Clark, J..Magn. Magn. Mater. 12, 233 (1979).
[41] P.J. Picone and P.E. Clark, J. Magn. Magn. Mater. 25 140 (1981).
[42] N. Kawamiya, K. Adachi, J. Phys. Soc. Jpn. 55, 2, 634 (1986).
[43] N. Kawamiya, K. Adachi, and Y. Nakamura, J. Phys. Soc. Jpn, 33, 5, 1318 (1972).
[44] J.M. Gaudet, T.D. Hatchard, S.P. Farrell, and R.A. Dunlap, J. Magn. Magn. Mater. 320, 821 (2008).